

$2M_1$ -phlogopite from Black Hills (South Australia): The first case of configurational polytype in micas

FERNANDO SCORDARI,* EMANUELA SCHINGARO, ERNESTO MESTO, AND MARIA LACALAMITA

Dipartimento di Scienze della Terra e Geoambientali, Università degli Studi di Bari, via E. Orabona 4, I-70125 Bari, Italy

ABSTRACT

The $2M_1$ -phlogopite from the potassic gabbro-norite (Black Hill, Australia) has been studied by electron microprobe and single-crystal X-ray diffraction analyses. The crystal-chemical formula was $(K_{0.95}Na_{0.01})(Al_{0.15}Mg_{1.27}Fe_{1.16}^{2+}Fe_{0.04}^{3+}Ti_{0.38}^{4+})(Si_{2.85}Al_{1.15})O_{10.76}F_{0.11}Cl_{0.03}OH_{1.10}$. The structural analysis has shown that the crystal has the cell parameters $a = 5.352(1)$, $b = 9.268(1)$, $c = 20.168(1)$ Å, and $\beta = 95.10(1)^\circ$ and exhibits symmetry lowering from the ideal space group $C2/c$ to $C1$. An octahedral cation ordering pattern was revealed from the refined site-scattering powers. Specifically, using the scattering species Mg vs. Fe, it was found that the M1 site at $z = 0$ was occupied principally by Mg (~77%) and subordinately by Fe (~23%), whereas that at $z = 0.5$ was completely occupied by Fe; the M2 sites at $z = 0$ displayed ~88% Mg and ~12% Fe, whereas those at $z = 0.5$ were occupied by ~86% Fe and ~14% Mg. The analysis of geometrical features shows that the Ti uptake in the structure via the Ti-oxy mechanism induces structural distortions of different extents on the $z = 0$ and $z = 0.5$ layers, with stronger effects for the layer at $z = 0$. Minor chemical and structural differences, instead, affect the T sheets at $z = 0$ and $z = 0.5$.

Keywords: $2M_1$ -phlogopite, octahedral cation ordering, symmetry lowering, structure refinement

INTRODUCTION

Trioctahedral micas are principally $1M$ polytype and only subordinately $2M_1$, $2M_2$, and $3T$ (Bailey 1984), whereas dioctahedral micas are prevalently $2M_1$ polytypes, although $3T$ and $1M$ structures have been found (Brigatti and Guggenheim 2002). For such a reason, polytype $2M_1$ in trioctahedral micas are comparatively less studied than the $1M$ polytype. The $2M_1$ polytype has ideally $C2/c$ symmetry.

The crystal-chemical features of $2M_1$ -biotites with $C2/c$ space group have been analyzed by several authors (for a review see Scordari et al. 2012 and references therein), whereas the cases of $2M_1$ trioctahedral micas with symmetry lowering have been less documented. Specifically, Takeda and Ross (1975) and Ohta et al. (1982) studied the coexistence of $1M$ and $2M_1$ polytypes in Ruiz Peak (New Mexico) oxy-biotite. They found that the unit layer of $2M_1$ polytype is characterized, relative to the unit layer of $1M$ polytype, by a shift along $\pm b$ of the upper and lower triads of octahedral oxygen atoms. As a consequence, the layer symmetry is better described in space group $C\bar{1}$. Other instances of $2M_1$ micas showing symmetry different from $C2/c$, namely Cc (Lin and Guggenheim 1983; Lahti and Saikkonen 1985; Rieder et al. 1996), $C1$ (Slade et al. 1987), $C\bar{1}$ (Swanson and Bailey 1981), Am (Bujnowski et al. 2009) are characterized by remarkably rare composition and/or cation ordering.

Lin and Guggenheim (1983) refined in space group Cc the structure of a mica specimen with composition intermediate

between a bityite- $2M_1$ and a margarite- $2M_1$, i.e., a trioctahedral and a dioctahedral mica, respectively. The nearly complete tetrahedral ordering of Al, Be relative to Si and the pattern that these atoms take on resulted in the violation of the center of symmetry of the $C2/c$ space group, leading to the final Cc symmetry. The authors also reported octahedral cation ordering (Li and vacancy partitioned at M1; Al at M2 and M3 octahedral sites, respectively) that, however, was not involved in the symmetry lowering. Lahti and Saikkonen (1985) document ordering of tetrahedral Si and Al+Be in bityite from pegmatites of the Eräjärvi area at Orivesi, Finland on the basis of the analysis of infrared absorption bands. By contrast, Rieder et al. (1996) analyzed zinnwaldite from mine Barbora, Krupka, Czech Republic, and found very low degree of tetrahedral ordering but remarkable octahedral ordering: Li and Fe^{2+} prefer M1 (M3) to M2, whereas Al does the opposite. Slade et al. (1987) refined the ephesite structure in space group $C1$. In this case, both tetrahedral and octahedral cation ordering was revealed. The presence of reflections violating the c glide plane and the occurrence of stacking disorder were also highlighted. Swanson and Bailey (1981) studying a lepidolite from Biskupice, Czech Republic, found the presence of some $h0l$ reflection pointing to a small deviation from the monoclinic symmetry $C2/c$ and concluded that the most likely space group of this mica was $C\bar{1}$ not on the basis of structure refinement but as a result of a second harmonic generation test.

In the present work, a $2M_1$ -phlogopite from potassic gabbro-norite plutons of the Black Hills region, south Australia, petrologically characterized by Turner (1996) is considered.

* E-mail: fernando.scordari@uniba.it

Coexistence of 1M and 2M₁ polytype in the same host rock has been documented, but the investigation on 1M polytype was reported elsewhere (see Schingaro et al. 2005). In the present work, the characterization of the 2M₁ polytype was accomplished by combination of chemical and structural analyses.

EXPERIMENTAL METHODS

The phlogopite analyzed here (labeled "BHG"), belongs to the Black Hills potassic gabbro-norite dated 489 ± 39 Ma, and formed under high-temperature (1200–1000 °C), low-pressure (~1 kbar), and moderate *f*_{o₂} conditions (Turner 1996). The crystal sample was investigated combining electron probe microanalysis (EPMA) and single-crystal X-ray diffraction (SCXRD).

Chemical composition was measured on the crystal embedded in epoxy resin and polished. A Cameca SX-50 electron microprobe operating at 15 kV accelerating voltage, 15 nA specimen beam current, and 10 μm beam diameter was used. The analyses were carried out with wavelength-dispersive spectrometers for Na, K, Ba, F, Cl, Ni, Ti, and Mn, and with energy-dispersive spectrometers for Si, Al, Mg, and Fe. The following standards were employed: jadeite (Na), orthoclase (K), barite (Ba), apatite (F), sylvite (Cl), nickeline (Ni), rutile (Ti), rhodonite (Mn), wollastonite (Si), corundum (Al), periclase (Mg), and magnetite (Fe). Data acquisition followed the procedure suggested by Foley (1989). A conversion from X-ray counts to oxide weight percentages (wt%) was carried out with the PAP method (Pouchou and Pichoir 1985). The relative analytical uncertainty is 1% for major elements and 4% for minor elements. Oxide weight percentages (wt%) averaged over 6 spots are reported in Table 1, also in comparison with those of the

TABLE 1. Chemical composition (oxide wt%): comparison between 1M- and 2M₁-BHG crystals

	2M ₁ -BHG	1M-BHG*
SiO ₂	35.7(3)	35.6(8)
Al ₂ O ₃	13.8(1)	13.9(3)
MgO	10.7(2)	10.7(4)
FeO	18.0(3)	18.5(8)
TiO ₂	6.3(2)	6.8(4)
MnO	0.06(4)	n.d.
NiO	0.02(2)	n.d.
K ₂ O	9.3(1)	9.4(1)
Na ₂ O	0.05(2)	0.02(2)
BaO	0.11(4)	0.02(2)
F	0.41(9)	0.0(1)
Cl	0.25(2)	0.27(5)
Total	94.7	95.2

Note: * from Schingaro et al. (2005); n.d. = not determined.

TABLE 2. Selected data about collection and refinements of the study crystal in C2/c, C $\bar{1}$, and C1 space groups

Crystal size (mm ³)	2M ₁ -BHG		
	C2/c	C $\bar{1}$	C1
Space group	C2/c	C $\bar{1}$	C1
<i>a</i> (Å)	5.352(1)		
<i>b</i> (Å)	9.268(1)		
<i>c</i> (Å)	20.168(1)		
β (°)	95.10(1)		
Cell volume (Å ³)	996.4(2)		
Z	4		
θ range for data collection	2 to 36°		
Reflections collected	23178		
Reflections unique	2389	4596	4596
<i>R</i> _{merging} (<i>R</i> _{int}) (%)	4.76	4.44	4.44
Reflections used [<i>I</i> > 5 σ (<i>I</i>)]	1429	2287	2318
Range of <i>h, k, l</i>	-8 ≤ <i>h</i> ≤ 8 -15 ≤ <i>k</i> ≤ 15 -33 ≤ <i>l</i> ≤ 33		
No. of refined parameters	76	211	283
Goof*	1.033	1.076	1.096
<i>R</i> ₁ † [on <i>F</i>] (%)	7.96	4.38	4.16
<i>wR</i> ₂ ‡ [on <i>F</i> ²] (%)	7.40	4.81	4.74
$\Delta\rho_{\min}/\Delta\rho_{\max}$ (e ⁻ /Å ³)	-2.63/2.02	-1.35/1.65	-0.83/1.59

* Goodness-of-fit = $\{\sum[w(F_o^2 - F_c^2)]^2 / (N - P)\}^{1/2}$, where *N* and *P* are the number of reflections and parameters, respectively.

† $R_1 = \sum[|F_o| - |F_c|] / \sum|F_o|$.

‡ $wR_2 = \{\sum[w(F_o^2 - F_c^2)]^2 / \sum[w(F_o^2)]\}^{1/2}$; *w* = Chebyshev optimized weights.

1M polytype (Schingaro et al. 2005).

X-ray intensity data collections were performed by means of a Bruker AXS D8 APEXII automated diffractometer operating at 55 kV and 30 mA, with graphite monochromatized MoK α (λ = 0.7107 Å) radiation. The collection strategy was optimized by the Apex program suite (Bruker 2003a). A total of 5400 frames were collected with ω and ϕ scan steps, scan width 0.2°, exposure time 10s/frame, detector-to-sample distance 5 cm. For the extraction of the reflection intensities and Lorentz-polarization corrections, the SAINT package was used (Bruker 2003b). A semi-empirical absorption correction was accomplished using the SADABS software (Sheldrick 2003); the structure refinements were performed with the program CRYSTALS (Betteridge et al. 2003). Initial refinement was carried out in the space group C2/c starting from the atomic coordinates of Ruiz Peak biotite (Ohta et al. 1982). Reflections with *I* > 5 σ (*I*) were used and the refined parameters were: scale factor, atomic positions, cation occupancies, and anisotropic atomic displacement parameters. Ionized X-ray scattering curves were used for interlayer and octahedral sites, whereas ionized vs. neutral species were employed for Si and O to better evaluate electron densities at these sites (Hawthorne et al. 1995).

However, the analysis of reflections via XPREP showed the presence of 468 *h*0*l* reflections that violated the systematic absences required by the *c*-glide plane, out of which 242 had *I*/ σ > 3. The mean intensity of these reflections was reported to be $\langle I \rangle = 38.3$, with $\langle I/\sigma \rangle = 4.8$. These data indicated a deviation from the C2/c symmetry. Therefore, further refinements were performed in different space groups as reported in the Results section below.

RESULTS

The studied crystal shows intra-crystalline homogeneity and its chemical composition (see Table 1) results very close to that of the 1M polytype from the same rock sample that has been previously analyzed by Schingaro et al. (2005).

In Table 2, the cell parameters of the studied crystal, *a* = 5.352(1), *b* = 9.268(1), *c* = 20.168(1) Å, and β = 95.10(1)° are typical of the 2M₁ polytype with ideal space group C2/c. The initial stage of the structure refinement was carried out in this space group. Therefore, the reflections violating the *c*-glide extinctions (XPREP analysis, see the Experimental section above) were neglected leaving 2389 unique reflections, out of which 1429 with *I* > 5 σ (*I*) were considered. Isotropic refinement with 61 refined parameters converged at *R*₁ = 9.94% and *wR*₂ = 9.51% but evidenced anomalously low isotropic displacement parameters for the O31 and O32 oxygen sites. Fully anisotropic refinement with 112 refined parameters yielded *R*₁ = 4.79% and *wR*₂ = 4.53% but showed non positive definite displacement parameters for the O31, O32, and O4 oxygen atoms. The best refinement in this space group (*R*₁ = 7.96, *wR*₂ = 7.40, number of refined parameters = 76, see Table 2) was obtained by allowing the cations to vary anisotropically and the anions to vary isotropically. In this case, however, the isotropic displacement parameters of the octahedral O atoms (in particular O31 and O32 atoms) still refined at values lower than expected (see Table 3), because they are about one half than that of O4 oxygen.

The structure refinement was then carried out in the C $\bar{1}$ space group. The refinement was restarted using initially the same geometrical constraints as occur in the C2/c space group, with occupancies being free to vary. All atoms were treated anisotropically. The independent reflections were 4596, out of which 2287 with *I* > 5 σ (*I*) were considered in the refinement, while the number of refined parameters was 129. The refinement converged at *R*₁ = 5.6, *wR*₂ = 6.0%, with $\rho_{\min} = -2.56$ and $\rho_{\max} = 1.84$ e⁻/Å³ with no anomalies in thermal parameters. At this stage, a cation ordering pattern was revealed from the analysis of the refined site-scattering powers. Specifically, for the M1 site, the position at *z* = 0.0 was almost fully occupied by Mg, whereas

TABLE 3. Crystallographic coordinates, occupancies, equivalent isotropic (\AA^2), and anisotropic displacement parameters from the structure refinement of the study crystal in the $C2/c$ space group

Site	Atom	x	y	z	Occupancy	$U_{\text{iso/equiv}}$	U_{11}	U_{22}	U_{33}	U_{23}	U_{13}	U_{12}
K	K ⁺	0	0.0844(2)	1/4	1.001(1)	0.0358	0.0305(8)	0.0283(8)	0.049(1)	0.0000	0.0034(8)	0.0000
M1	Mg ²⁺	3/4	1/4	0	0.45(2)	0.0110	0.0085(5)	0.0092(6)	0.0157(7)	0.0000	0.0026(4)	0.0000
	Fe ²⁺	3/4	1/4	0	0.56(1)	0.0110	0.0085(5)	0.0092(6)	0.0157(7)	0.0000	0.0026(4)	0.0000
M2	Mg ²⁺	0.2435(2)	0.0813(1)	-0.00001(4)	0.54(2)	0.0123	0.0124(4)	0.0101(4)	0.0145(5)	0.0030(4)	0.0012(3)	0.0051(3)
	Fe ²⁺	0.2435(2)	0.0813(1)	-0.00001(4)	0.46(1)	0.0123	0.0124(4)	0.0101(4)	0.0145(5)	0.0030(4)	0.0012(3)	0.0051(3)
T1	Si, Si ⁴⁺	0.4624(2)	0.2505(1)	0.13768(7)	1.0(1)	0.0102	0.0064(4)	0.0084(5)	0.0158(6)	-0.0012(5)	0.0014(4)	0.0021(4)
T2	Si, Si ⁴⁺	0.9639(2)	0.4177(1)	0.13749(6)	1.0(1)	0.0120	0.0108(5)	0.0114(5)	0.0141(5)	-0.0016(6)	0.0018(3)	0.0031(5)
O11	O, O ²⁻	0.7386(7)	0.3184(4)	0.1653(2)	1.0(2)	0.0194(7)	-	-	-	-	-	-
O21	O, O ²⁻	0.2374(7)	0.3480(4)	0.1667(2)	1.0(2)	0.0199(7)	-	-	-	-	-	-
O22	O, O ²⁻	0.4430(6)	0.0845(4)	0.1665(2)	1.0(2)	0.0192(6)	-	-	-	-	-	-
O31	O, O ²⁻	0.4307(5)	0.2620(3)	0.0543(2)	1.0(2)	0.0089(5)	-	-	-	-	-	-
O32	O, O ²⁻	0.9384(5)	0.4303(3)	0.0547(1)	1.0(2)	0.0078(5)	-	-	-	-	-	-
O4	O, O ²⁻	0.9364(6)	0.0949(4)	0.0514(2)	1.0(2)	0.0130(5)	-	-	-	-	-	-

the position at $z = 0.5$ was fully occupied by Fe. Likewise, for the M2 site, the position at $z = 0$ displayed full occupancy of Mg scattering species, whereas the position at $z = 0.5$ was populated predominantly by Fe (~99%) and only ~1% by Mg. It was apparent from the analysis of site occupancies that those cation sites that were symmetry equivalent in the former $C2/c$ space group were no longer equivalent because of cation ordering. The following step was to relax the geometrical constraints of the $C2/c$ space group. The number of parameters increased to 211, taking into account that the displacement parameters of atoms previously equivalent by symmetry were constrained to be equal. The refinement converged at $R_1 = 4.38$ and $wR_2 = 4.81\%$ (see Table 2) but the equivalent isotropic displacement parameters for the O31, O31^[2], O32, and O32^[2] atoms were still lower than expected (see Table 4). However, attempts to release the constraints on anisotropic displacement parameter resulted in octahedral oxygen atoms to go negative. The final difference Fourier map gave $\rho_{\text{min}} = -1.35$ and $\rho_{\text{max}} = 1.65 \text{ e}/\text{\AA}^3$, the most intense occurring close to the M1 atom. Relevant cation-anion bond lengths as determined by structure refinement in the $C\bar{1}$ space group are given in Table 5.

It was then hypothesized that because of the cation ordering and of the different steric and charge features of the substituting

cations (Fe, Mg, and Ti above all) these atoms could shift from the ideal position (for instance M1 cation from the center of symmetry), so that refinement in space group $C1$ was attempted. As a first step, the geometrical constraints of space group $C2/c$ were kept for all atoms but no convergence was obtained.

In the next step, a partial anisotropic refinement was performed, without geometrical constraints, refining isotropically the thermal parameters of the oxygen atoms. $R_1 = 4.61$ and $wR_2 = 5.23$ values were obtained using 2318 reflections and refining 223 parameters. No anomalies in isotropic equivalent displacement parameters were observed. A full anisotropic refinement was then carried out with 2318 reflections with $I > 5\sigma(I)$, and 283 refined parameters, in full matrix mode, using damping factors for atoms coordinates and occupancies. The N/p (number of reflection/number of parameter) lowered from 10 to 8, the refinement converged at $R_1 = 4.16\%$, $wR_2 = 4.74$ and difference Fourier synthesis yielded $\rho_{\text{min}} = -0.83$ and $\rho_{\text{max}} = 1.59 \text{ e}/\text{\AA}^3$ (see Table 2). Displacement of the M1 cation was observed from the ideal position at ($3/4, 1/4, 1/2$) and a slight deviation from centrosymmetry for most atoms (Table 6). Standard deviations of atomic positions were slightly higher than those refined in space group $C\bar{1}$ (compare Tables 4 and 6).

In conclusion, the values of agreement indexes, bond length

TABLE 4. Crystallographic coordinates, occupancies, equivalent isotropic (\AA^2) and anisotropic displacement parameters from the structure refinement of the study crystal in the $C\bar{1}$ space group

Site	Atom	x	y	z	Occupancy	$U_{\text{iso/equiv}}$	U_{11}	U_{22}	U_{33}	U_{23}	U_{13}	U_{12}
K	K ⁺	-0.0005(2)	0.0843(1)	0.24990(8)	1.0189(9)	0.0370	0.0309(5)	0.0305(5)	0.0495(7)	-0.0001(4)	0.0033(4)	-0.0001(4)
M1	Mg ²⁺	3/4	1/4	0	0.8977(8)	0.0117	0.0105(6)	0.0116(6)	0.013(1)	-0.0012(6)	0.0024(6)	-0.0013(5)
	Fe ²⁺	3/4	1/4	0	0.1023(8)	0.0117	0.0105(6)	0.0116(6)	0.013(1)	-0.0012(6)	0.0024(6)	-0.0013(5)
M1 ^[2]	Fe ²⁺	1/4	1/4	1/2	1.0005(7)	0.0103	0.0075(3)	0.0068(3)	0.0167(5)	0.0011(3)	0.0026(3)	0.0020(2)
M2	Mg ²⁺	0.2390(2)	0.0798(1)	-0.00001(6)	1.0002(7)	0.0132	0.0150(6)	0.0130(5)	0.012(1)	0.0006(5)	0.0002(6)	-0.0008(2)
M2 ^[2]	Mg ²⁺	-0.24546(9)	0.08188(5)	0.49997(3)	0.0868(8)	0.0115	0.0102(2)	0.0079(2)	0.0166(4)	-0.0006(2)	0.0016(2)	-0.0008(2)
	Fe ²⁺	-0.24546(9)	0.08188(5)	0.49997(3)	0.9131(8)	0.0115	0.0102(2)	0.0079(2)	0.0166(4)	-0.0006(2)	0.0016(2)	-0.0008(2)
T1	Si ⁴⁺ , Si	0.4630(2)	0.2499(1)	0.13771(6)	0.995(1)	0.0118	0.0106(4)	0.0125(4)	0.0123(5)	-0.0001(4)	0.0009(4)	-0.0003(3)
T1 ^[2]	Si ⁴⁺ , Si	-0.4617(1)	0.25022(9)	0.36246(6)	0.989(1)	0.0085	0.0034(3)	0.0038(3)	0.0183(6)	-0.0004(3)	0.0016(3)	-0.0008(3)
T2	Si ⁴⁺ , Si	0.9651(2)	0.4172(1)	0.13766(6)	0.995(1)	0.0150	0.0169(5)	0.0178(5)	0.0102(6)	0.0000(4)	0.0009(4)	0.0006(4)
T2 ^[2]	Si ⁴⁺ , Si	-0.9626(2)	0.41704(9)	0.36252(6)	0.985(1)	0.0092	0.0052(4)	0.0045(4)	0.0183(7)	-0.0004(4)	0.0023(4)	-0.0002(3)
O11	O ²⁻ , O	0.7372(4)	0.3192(3)	0.1654(2)	0.3255(7)	0.0205	0.017(1)	0.026(1)	0.018(1)	0.002(1)	0.000(1)	-0.004(1)
O11 ^[2]	O ²⁻ , O	-0.7382(4)	0.3188(3)	0.3345(2)	0.4462(7)	0.0197	0.015(1)	0.024(1)	0.020(2)	-0.002(1)	0.001(1)	0.009(1)
O21	O ²⁻ , O	0.2378(4)	0.3479(3)	0.1666(2)	0.4798(7)	0.0208	0.016(1)	0.027(1)	0.019(2)	-0.001(1)	0.001(1)	0.004(1)
O21 ^[2]	O ²⁻ , O	-0.2379(4)	0.3489(3)	0.3336(2)	0.3359(7)	0.0198	0.016(1)	0.020(1)	0.023(2)	0.002(1)	0.001(1)	-0.009(1)
O22	O ²⁻ , O	0.4438(5)	0.0839(3)	0.1662(2)	0.3506(7)	0.0209	0.028(2)	0.016(1)	0.020(2)	-0.0005(1)	0.006(1)	0.000(1)
O22 ^[2]	O ²⁻ , O	-0.4428(5)	0.0843(3)	0.3334(2)	0.2173(7)	0.0195	0.029(1)	0.010(1)	0.021(2)	0.000(1)	0.005(1)	0.000(1)
O31	O ²⁻ , O	0.4322(4)	0.2504(3)	0.0552(2)	0.6198(7)	0.0189	0.021(1)	0.020(1)	0.016(2)	0.000(1)	0.003(1)	-0.002(1)
O31 ^[2]	O ²⁻ , O	-0.4296(4)	0.2499(2)	0.4459(2)	0.4898(7)	0.0090	0.0061(9)	0.0069(9)	0.014(1)	0.0013(8)	0.0022(9)	0.0013(7)
O32	O ²⁻ , O	0.9413(4)	0.4191(3)	0.0555(2)	0.4229(7)	0.0190	0.019(1)	0.022(1)	0.016(2)	-0.001(1)	0.001(1)	-0.001(1)
O32 ^[2]	O ²⁻ , O	-0.9358(4)	0.4187(2)	0.4458(2)	0.5837(7)	0.0085	0.0042(8)	0.0054(8)	0.016(2)	0.0001(8)	0.0031(9)	0.0016(7)
O41	O ²⁻ , O	0.9388(4)	0.0815(3)	0.0516(2)	0.5853(7)	0.0219	0.021(1)	0.019(1)	0.025(2)	-0.001(1)	0.004(1)	0.002(1)
O41 ^[2]	O ²⁻ , O	-0.9346(4)	0.0821(3)	0.4487(2)	0.8919(7)	0.0173	0.016(1)	0.015(1)	0.021(2)	-0.001(1)	0.000(1)	-0.0002(9)

Note: Superscript ^[2] indicates atomic position obtained by the twofold symmetry operation.

TABLE 5. Selected bond distances (Å) as determined by structure refinement in the C $\bar{1}$ space group

2M ₁ -BHG			
T1 tetrahedron			
T1-O11	1.653(3)	T1 ^[2] -O11 ^[2]	1.662(3)
T1-O21	1.655(3)	T1 ^[2] -O21 ^[2]	1.653(3)
T1-O22	1.649(3)	T1 ^[2] -O22 ^[2]	1.652(3)
T1-O31	1.659(4)	T1 ^[2] -O31 ^[2]	1.675(3)
<T1-O>	1.654	<T1 ^[2] -O>	1.661
T2 tetrahedron			
T2-O11	1.657(3)	T2 ^[2] -O11 ^[2]	1.647(3)
T2-O21	1.653(3)	T2 ^[2] -O21 ^[2]	1.660(3)
T2-O22	1.656(3)	T2 ^[2] -O22 ^[2]	1.664(3)
T2-O32	1.650(4)	T2 ^[2] -O32 ^[2]	1.673(3)
<T2-O>	1.654	<T2 ^[2] -O>	1.661
M1 octahedron			
M1-O31 (×2)	2.114(3)	M1 ^[2] -O31 ^[2] (×2)	2.113(2)
M1-O32 (×2)	2.134(3)	M1 ^[2] -O32 ^[2] (×2)	2.106(2)
M1-O41 (×2)	2.087(3)	M1 ^[2] -O41 ^[2] (×2)	2.070(3)
<M1-O>	2.112	<M1 ^[2] -O>	2.096
M2 octahedron			
M2-O31	2.091(3)	M2 ^[2] -O31 ^[2]	2.080(3)
M2-O31	2.146(3)	M2 ^[2] -O31 ^[2]	2.098(2)
M2-O32	2.104(3)	M2 ^[2] -O32 ^[2]	2.079(3)

TABLE 5.—CONTINUED

M2-O32	2.126(3)	M2 ^[2] -O32 ^[2]	2.108(2)
M2-O41	1.988(3)	M2 ^[2] -O41 ^[2]	2.033(3)
M2-O41	2.011(3)	M2 ^[2] -O41 ^[2]	2.037(3)
<M2-O>	2.078	<M2 ^[2] -O>	2.073
Interlayer			
K-O11		K-O11	3.032(3)
K-O11		K-O11	3.308(3)
K-O11 ^[2]		K-O11 ^[2]	3.030(3)
K-O11 ^[2]		K-O11 ^[2]	3.312(3)
K-O21		K-O21	3.028(3)
K-O21		K-O21	3.287(3)
K-O21 ^[2]		K-O21 ^[2]	3.027(3)
K-O21 ^[2]		K-O21 ^[2]	3.296(3)
K-O22		K-O22	3.036(3)
K-O22		K-O22	3.287(3)
K-O22 ^[2]		K-O22 ^[2]	3.024(3)
K-O22 ^[2]		K-O22 ^[2]	3.294(3)
<K-O> _{inner}		<K-O> _{inner}	3.030
<K-O> _{outer}		<K-O> _{outer}	3.297
<K-O> _{outer}		<K-O> _{outer}	3.164

Note: Superscript ^[2] indicates atomic position obtained by the twofold symmetry operation.

TABLE 6. Crystallographic coordinates, occupancies, equivalent isotropic (Å^2) and anisotropic displacement parameters from the structure refinement of the study crystal in the C1 space group

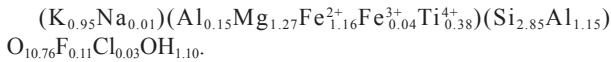
Site	Atom	x	y	z	Occupancy	$U_{\text{iso/equiv}}$	U_{11}	U_{22}	U_{33}	U_{23}	U_{13}	U_{12}
K	K ⁺	-0.0150(5)	0.0842(3)	0.2500(3)	1.026(3)	0.0366	0.0311(5)	0.0306(5)	0.0480(6)	0.0003(4)	0.0029(4)	-0.0006(4)
K ⁽¹⁾	K ⁺	-0.0139(5)	-0.0848(3)	0.7499(2)	1.028(3)	0.0366	0.0311(5)	0.0306(5)	0.0480(6)	0.0003(4)	0.0029(4)	-0.0006(4)
M1	Mg ²⁺	3/4	1/4	0	0.768(2)	0.0107	0.0070(3)	0.0081(3)	0.0175(3)	0.0000(3)	0.0032(3)	0.0017(2)
	Fe ²⁺	3/4	1/4	0	0.232(2)	0.0107	0.0070(3)	0.0081(3)	0.0175(3)	0.0000(3)	0.0032(3)	0.0017(2)
M1 ^[2]	Fe ²⁺	0.2369(4)	0.2411(2)	0.4996(2)	0.9990(9)	0.0107	0.0070(3)	0.0081(3)	0.0175(3)	0.0000(3)	0.0032(3)	0.0017(2)
M2	Mg ²⁺	0.2074(4)	0.0798(3)	0.0004(2)	0.833(2)	0.0106	0.0102(7)	0.0080(5)	0.0134(6)	0.0020(4)	0.0003(6)	0.0060(5)
	Fe ²⁺	0.2074(4)	0.0798(3)	0.0004(2)	0.167(2)	0.0106	0.0102(7)	0.0080(5)	0.0134(6)	0.0020(4)	0.0003(6)	0.0060(5)
M2 ⁽¹⁾	Mg ²⁺	-0.2756(4)	-0.0808(3)	0.0006(2)	0.930(2)	0.0106	0.0102(7)	0.0080(5)	0.0134(6)	0.0020(4)	0.0003(6)	0.0060(5)
	Fe ²⁺	-0.2756(4)	-0.0808(3)	0.0006(2)	0.070(2)	0.0106	0.0102(7)	0.0080(5)	0.0134(6)	0.0020(4)	0.0003(6)	0.0060(5)
M2 ^[2]	Mg ²⁺	-0.2592(3)	0.0725(2)	0.5001(2)	0.172(2)	0.0105	0.0080(2)	0.0077(2)	0.0161(3)	-0.0008(2)	0.0017(2)	-0.0020(2)
	Fe ²⁺	-0.2592(3)	0.0725(2)	0.5001(2)	0.828(2)	0.0105	0.0080(2)	0.0077(2)	0.0161(3)	-0.0008(2)	0.0017(2)	-0.0020(2)
M2 ^(c)	Mg ²⁺	0.2315(3)	-0.0907(2)	0.5000(2)	0.119(2)	0.0105	0.0080(2)	0.0077(2)	0.0161(3)	-0.0008(2)	0.0017(2)	-0.0020(2)
	Fe ²⁺	0.2315(3)	-0.0907(2)	0.5000(2)	0.881(2)	0.0105	0.0080(2)	0.0077(2)	0.0161(3)	-0.0008(2)	0.0017(2)	-0.0020(2)
T1	Si ⁴⁺ , Si	0.4478(4)	0.2522(3)	0.1386(2)	0.996(2)	0.0100	0.0110(4)	0.0061(4)	0.0129(5)	-0.0003(4)	0.0003(4)	-0.0003(3)
T1 ⁽¹⁾	Si ⁴⁺ , Si	-0.4792(4)	-0.2478(3)	-0.1366(2)	1.000(2)	0.0100	0.0110(4)	0.0061(4)	0.0129(5)	-0.0003(4)	0.0003(4)	-0.0003(3)
T1 ^[2]	Si ⁴⁺ , Si	-0.4787(4)	0.2451(3)	0.3629(2)	0.995(2)	0.0090	0.0044(3)	0.0060(4)	0.0165(5)	-0.0005(4)	0.0013(3)	-0.0013(3)
T1 ^(c)	Si ⁴⁺ , Si	0.4446(4)	-0.2551(3)	0.6381(2)	0.999(2)	0.0090	0.0044(3)	0.0060(4)	0.0165(5)	-0.0005(4)	0.0013(3)	-0.0013(3)
T2	Si ⁴⁺ , Si	0.9515(4)	0.4194(3)	0.1376(2)	1.000(2)	0.0120	0.0147(5)	0.0087(5)	0.0126(5)	0.0005(5)	0.0011(4)	0.0006(4)
T2 ⁽¹⁾	Si ⁴⁺ , Si	-0.9792(4)	-0.4150(3)	-0.1374(2)	1.000(2)	0.0120	0.0147(5)	0.0087(5)	0.0126(5)	0.0005(5)	0.0011(4)	0.0006(4)
T2 ^[2]	Si ⁴⁺ , Si	-0.9784(4)	0.4108(3)	0.3633(2)	1.000(2)	0.0096	0.0060(4)	0.0079(4)	0.0152(5)	-0.0004(4)	0.0027(4)	-0.0009(3)
T2 ^(c)	Si ⁴⁺ , Si	0.9453(4)	-0.4234(3)	0.6383(2)	0.993(2)	0.0096	0.0060(4)	0.0079(4)	0.0152(5)	-0.0004(4)	0.0027(4)	-0.0009(3)
O11	O, O ²⁻	0.7256(6)	0.3220(5)	0.1668(4)	1.000(2)	0.0196	0.018(1)	0.022(1)	0.019(1)	0.002(1)	0.002(1)	-0.006(1)
O11 ⁽¹⁾	O, O ²⁻	-0.7492(6)	-0.3166(5)	-0.1644(4)	1.000(2)	0.0196	0.018(1)	0.022(1)	0.019(1)	0.002(1)	0.002(1)	-0.006(1)
O11 ^[2]	O, O ²⁻	-0.7549(6)	0.3135(5)	0.3350(4)	1.000(2)	0.0192	0.017(1)	0.022(1)	0.019(1)	-0.003(1)	0.001(1)	0.007(1)
O11 ^(c)	O, O ²⁻	0.7214(6)	-0.3247(5)	0.6660(4)	1.000(2)	0.0192	0.017(1)	0.022(1)	0.019(1)	-0.003(1)	0.001(1)	0.007(1)
O21	O, O ²⁻	0.2234(6)	0.3545(5)	0.1672(4)	1.000(2)	0.0179	0.017(1)	0.018(1)	0.019(1)	-0.001(1)	-0.000(1)	0.005(1)
O21 ⁽¹⁾	O, O ²⁻	-0.2513(6)	-0.3419(5)	-0.1659(4)	1.000(2)	0.0179	0.017(1)	0.018(1)	0.019(1)	-0.001(1)	-0.000(1)	0.005(1)
O21 ^[2]	O, O ²⁻	-0.2568(6)	0.3417(5)	0.3348(4)	1.000(2)	0.0183	0.016(1)	0.020(1)	0.020(1)	0.002(1)	0.000(1)	-0.010(1)
O21 ^(c)	O, O ²⁻	0.2188(6)	-0.3555(5)	0.6673(4)	1.000(2)	0.0183	0.016(1)	0.020(1)	0.020(1)	0.002(1)	0.000(1)	-0.010(1)
O22	O, O ²⁻	0.4274(6)	0.0896(4)	0.1652(4)	1.000(2)	0.0177	0.026(1)	0.008(1)	0.019(1)	0.002(1)	0.004(1)	0.002(1)
O22 ⁽¹⁾	O, O ²⁻	-0.4612(6)	-0.0788(4)	-0.1674(4)	1.000(2)	0.0177	0.026(1)	0.008(1)	0.019(1)	0.002(1)	0.004(1)	0.002(1)
O22 ^[2]	O, O ²⁻	-0.4616(6)	0.0797(4)	0.3346(4)	1.000(2)	0.0192	0.029(2)	0.010(1)	0.020(1)	0.000(1)	0.008(1)	-0.002(1)
O22 ^(c)	O, O ²⁻	0.4245(6)	-0.0894(5)	0.6674(4)	1.000(2)	0.0192	0.029(2)	0.010(1)	0.020(1)	0.000(1)	0.008(1)	-0.002(1)
O31	O, O ²⁻	0.4101(6)	0.2509(5)	0.0567(4)	1.000(2)	0.0137	0.015(1)	0.012(1)	0.014(1)	-0.001(1)	0.002(1)	0.0040(9)
O31 ⁽¹⁾	O, O ²⁻	-0.4558(6)	-0.2479(5)	-0.0543(4)	1.000(2)	0.0137	0.015(1)	0.012(1)	0.014(1)	-0.001(1)	0.002(1)	0.0040(9)
O31 ^[2]	O, O ²⁻	-0.4474(5)	0.2386(4)	0.4456(4)	1.000(2)	0.0103	0.0077(9)	0.009(1)	0.015(1)	-0.001(1)	0.004(1)	-0.0009(8)
O31 ^(c)	O, O ²⁻	0.4086(5)	-0.2607(4)	0.5535(4)	1.000(2)	0.0103	0.0077(9)	0.009(1)	0.015(1)	-0.001(1)	0.004(1)	-0.0009(8)
O32	O, O ²⁻	0.9185(6)	0.4185(5)	0.0564(4)	1.000(2)	0.0133	0.012(1)	0.012(1)	0.015(1)	-0.000(1)	0.000(1)	0.0047(9)
O32 ⁽¹⁾	O, O ²⁻	-0.9631(6)	-0.4196(5)	-0.0549(4)	1.000(2)	0.0133	0.012(1)	0.012(1)	0.015(1)	-0.000(1)	0.000(1)	0.0047(9)
O32 ^[2]	O, O ²⁻	-0.9573(5)	0.4097(5)	0.4444(4)	1.000(2)	0.0103	0.0058(9)	0.012(1)	0.013(2)	-0.002(1)	0.002(1)	-0.0026(8)
O32 ^(c)	O, O ²⁻	0.9148(5)	-0.4280(5)	0.5529(4)	1.000(2)	0.0103	0.0058(9)	0.012(1)	0.013(2)	-0.002(1)	0.002(1)	-0.0026(8)
O41	O, O ²⁻	0.9100(6)	0.0797(5)	0.0516(4)	1.000(2)	0.0148	0.011(1)	0.014(1)	0.020(2)	0.001(1)	-0.002(1)	0.006(1)
O41 ⁽¹⁾	O, O ²⁻	-0.9681(6)	-0.0821(5)	-0.0526(4)	1.000(2)	0.0148	0.011(1)	0.014(1)	0.020(2)	0.001(1)	-0.002(1)	0.006(1)
O41 ^[2]	O, O ²⁻	-0.9545(6)	0.0717(5)	0.4488(4)	1.000(2)	0.0144	0.012(1)	0.013(1)	0.018(2)	-0.001(1)	0.001(1)	-0.0031(9)
O41 ^(c)	O, O ²⁻	0.9131(6)	-0.0903(5)	0.5502(4)	1.000(2)	0.0144	0.012(1)	0.013(1)	0.018(2)	-0.001(1)	0.001(1)	-0.0031(9)

Note: Superscript ^[2] indicates atomic position obtained by the twofold symmetry operation; superscript ⁽¹⁾ indicates atomic position obtained by inversion center; superscript ^(c) indicates atomic position obtained by the c-glide.

distances and mean atomic number were generally similar for the structure refinements in both $C1$ and $C\bar{1}$ space groups (see Tables 2 and 8, and compare Tables 5 and 7). However, the structural model in $C1$ space group appears more consistent with crystal-chemical considerations about cation ordering in the $z = 0.0$ and $z = 0.5$ layer (see the Discussion and Conclusion section below).

DISCUSSION AND CONCLUSION

The EPMA (see Table 1) and SCXRD data were combined with the Mössbauer results [$^{57}\text{Fe}^{2+} = 97.0(7)$; $^{57}\text{Fe}^{3+} = 3.0(7)$] reported in the $1M$ -BHG phlogopite study (see Schingaro et al. 2005) and OH^- content geometrically estimated basing on the c vs. OH^- relationship for $2M_1$ micas (Scordari et al. 2012) to calculate, on the basis of $(\text{O}_{12-x-y-z}\text{OH}_x\text{Cl}_y\text{F}_z)$, the following structural formula:



The Ti was considered all belonging to the tetravalent species

TABLE 7. Selected bond distances (Å) as determined by structure refinement in the $C1$ space group

$2M_1$ -BHG							
T1 Tetrahedron							
T1-O11	1.674(4)	T1 ^(f) -O11 ^(f)	1.633(4)	T1 ⁽²⁾ -O11 ⁽²⁾	1.660(4)	T1 ^(c) -O11 ^(c)	1.667(4)
T1-O21	1.672(5)	T1 ^(f) -O21 ^(f)	1.652(5)	T1 ⁽²⁾ -O21 ⁽²⁾	1.628(5)	T1 ^(c) -O21 ^(c)	1.673(5)
T1-O22	1.607(5)	T1 ^(f) -O22 ^(f)	1.691(5)	T1 ⁽²⁾ -O22 ⁽²⁾	1.642(5)	T1 ^(c) -O22 ^(c)	1.652(5)
T1-O31	1.646(9)	T1 ^(f) -O31 ^(f)	1.654(9)	T1 ⁽²⁾ -O31 ⁽²⁾	1.662(8)	T1 ^(c) -O31 ^(c)	1.701(8)
<T1-O>	1.645	<T1 ^(f) -O>	1.658	<T1 ⁽²⁾ -O>	1.648	<T1 ^(c) -O>	1.673
T2 Tetrahedron							
T2-O11	1.658(5)	T2 ^(f) -O11 ^(f)	1.661(5)	T2 ⁽²⁾ -O11 ⁽²⁾	1.640(5)	T2 ^(c) -O11 ^(c)	1.644(5)
T2-O21	1.638(4)	T2 ^(f) -O21 ^(f)	1.662(4)	T2 ⁽²⁾ -O21 ⁽²⁾	1.675(4)	T2 ^(c) -O21 ^(c)	1.652(4)
T2-O22	1.681(6)	T2 ^(f) -O22 ^(f)	1.639(6)	T2 ⁽²⁾ -O22 ⁽²⁾	1.674(5)	T2 ^(c) -O22 ^(c)	1.654(5)
T2-O32	1.631(9)	T2 ^(f) -O32 ^(f)	1.660(9)	T2 ⁽²⁾ -O32 ⁽²⁾	1.629(8)	T2 ^(c) -O32 ^(c)	1.716(8)
<T2-O>	1.652	<T2 ^(f) -O>	1.656	<T2 ⁽²⁾ -O>	1.655	<T2 ^(c) -O>	1.667
M1 Octahedron							
M1-O31	2.233(5)	M1 ⁽²⁾ -O31 ⁽²⁾	2.091(6)	M1 ^(c) -O31 ^(c)	2.147(6)		
M1-O31 ^(f)	1.996(5)	M1 ⁽²⁾ -O31 ^(c)	2.147(6)				
M1-O32	2.089(5)	M1 ⁽²⁾ -O32 ⁽²⁾	2.134(5)				
M1-O32 ^(f)	2.185(5)	M1 ⁽²⁾ -O32 ^(c)	2.083(6)				
M1-O41	2.037(5)	M1 ⁽²⁾ -O41 ⁽²⁾	2.092(6)				
M1-O41 ^(f)	2.165(5)	M1 ⁽²⁾ -O41 ^(c)	2.050(6)				
<M1-O>	2.118	<M1 ⁽²⁾ -O>	2.100				
M2 Octahedron							
M2-O31	2.182(6)	M2 ^(f) -O31	2.121(6)	M2 ⁽²⁾ -O31 ⁽²⁾	2.097(5)	M2 ^(c) -O31 ⁽²⁾	2.107(5)
M2-O31 ^(f)	2.088(6)	M2 ^(f) -O31 ^(f)	2.089(6)	M2 ⁽²⁾ -O31 ^(c)	2.047(5)	M2 ^(c) -O31 ^(c)	2.089(5)
M2-O32	2.136(5)	M2 ^(f) -O32	2.068(6)	M2 ⁽²⁾ -O32 ⁽²⁾	2.110(5)	M2 ^(c) -O32 ⁽²⁾	2.089(5)
M2-O32 ^(f)	2.169(6)	M2 ^(f) -O32 ^(f)	2.072(6)	M2 ⁽²⁾ -O32 ^(c)	2.124(5)	M2 ^(c) -O32 ^(c)	2.046(5)
M2-O41	1.972(6)	M2 ^(f) -O41	2.019(6)	M2 ⁽²⁾ -O41 ⁽²⁾	2.007(6)	M2 ^(c) -O41 ⁽²⁾	2.035(5)
M2-O41 ^(f)	2.024(6)	M2 ^(f) -O41 ^(f)	2.043(6)	M2 ⁽²⁾ -O41 ^(c)	1.996(5)	M2 ^(c) -O41 ^(c)	2.058(5)
<M2-O>	2.095	<M2 ^(f) -O>	2.069	<M2 ⁽²⁾ -O>	2.064	<M2 ^(c) -O>	2.071
Interlayer							
K-O11	3.031(6)	K ^(f) -O11 ^(f)	3.029(6)				
K-O11	3.280(6)	K ^(f) -O11 ^(f)	3.337(6)				
K-O11 ⁽²⁾	2.996(6)	K ^(f) -O11 ^(c)	3.064(6)				
K-O11 ⁽²⁾	3.358(6)	K ^(f) -O11 ^(c)	3.262(6)				
K-O21	2.977(6)	K ^(f) -O21 ^(f)	3.082(6)				
K-O21	3.327(6)	K ^(f) -O21 ^(f)	3.249(6)				
K-O21 ⁽²⁾	3.077(6)	K ^(f) -O21 ^(c)	2.986(6)				
K-O21 ⁽²⁾	3.271(7)	K ^(f) -O21 ^(c)	3.315(6)				
K-O22	3.041(6)	K ^(f) -O22 ^(f)	3.037(6)				
K-O22	3.305(5)	K ^(f) -O22 ^(f)	3.265(5)				
K-O22 ⁽²⁾	3.058(6)	K ^(f) -O22 ^(c)	2.995(6)				
K-O22 ⁽²⁾	3.285(5)	K ^(f) -O22 ^(c)	3.304(5)				
<K-O> _{inner}	3.030	<K ^(f) -O> _{inner}	3.032				
<K-O> _{outer}	3.304	<K ^(f) -O> _{outer}	3.288				
<K-O>	3.167	<K ^(f) -O>	3.160				

Note: Superscript ⁽²⁾ indicates atomic position obtained by the twofold symmetry operation; superscript ^(f) indicates atomic position obtained by inversion center; superscript ^(c) indicates atomic position obtained by the c -glide.

according to recent developments of data analysis based on a more rigorous treatment of the background for X-ray photoelectron spectra of BHG- $1M$ crystals (Castle and Salvi 2001; Mesto et al. 2008).

The structural formula, above, is also in agreement with the X-ray data (see Table 8) and is balanced by the following substitution mechanisms: Al , Fe^{3+} -Tschermak [$^{VI}\text{M}^{2+} + ^{IV}\text{Si}^{4+} \leftrightarrow ^{VI}\text{M}^{3+} + ^{IV}\text{Al}^{3+}$]; Ti-oxy [$^{VI}\text{M}^{2+} + 2(\text{OH})^- \leftrightarrow ^{VI}\text{Ti}^{4+} + 2(\text{O}^{2-}) + \text{H}_2\uparrow$]; and $^{XII}\text{K}^+ + ^{IV}\text{Al}^{3+} \leftrightarrow ^{IV}\text{Si}^{4+} + ^{XII}\text{Cl}$.

In comparison to all the other literature $2M_1$ micas (Scordari et al. 2012 and references therein), in the classification plot of Figure 1 the study $2M_1$ -BHG mica follows the general trend, showing a slight deviation toward the annite end-member.

The sketch shown in Figure 2 illustrates the structural features of the study crystal. The analysis of the details of the TOT layer at $z = 0$ as compared with the TOT layer at $z = 0.5$ evidences that:

(1) An octahedral ordering is clearly apparent from a chemical viewpoint, i.e., if refined site-scattering powers are taken into account. This can be seen from the comparison of the occupancies for the sites M1, M2 (Mg-rich) and M1⁽²⁾, M2⁽²⁾ (Fe-rich) in $C\bar{1}$ space group (see Table 4) and for the sites M1, M2, M2^(f) (Mg-rich) and M1⁽²⁾, M2⁽²⁾, M2^(c) (Fe-rich) in $C1$ space group (see Table 6). As a further detail, scattering power at M2 site in $C\bar{1}$ refines to 12 e^- , whereas in $C1$ M2 refines to 14.34 and M2^(f) to 12.98 e^- with a difference of 1.36 e^- , which indicates significantly different chemical content in the latter two sites. From a geometrical viewpoint (i.e., average bond distances and octahedral volumes), there seems to be no evidence of octahedral ordering. For instance, $\langle\text{M-O}\rangle_{z=0}$ is slightly larger than $\langle\text{M-O}\rangle_{z=0.5}$ (see Tables 5 and 7) despite the fact that the former site is predominantly occupied by Mg (ionic radius 0.72 Å from Shannon 1976) and the latter by Fe^{2+} (ionic radius 0.78 Å from Shannon 1976). This may be due to the covalent character of the Fe-O as to the Mg-O bonds.

The octahedral cation distributions for both $C\bar{1}$ and $C1$ space groups give good agreement (i.e., differences are within ~ 0.5 e^- /site) between mean atomic numbers as assessed by chemical determinations and structure refinement (see Table 9). However, note that the octahedral cation partitioning for the $C\bar{1}$ space group provides 0.16 and 0.60 Ti atoms per formula unit (apfu) at $z = 0$ and $z = 0.5$ layer, respectively. Conversely, the proposed cation distribution for the $C1$ space group gives 0.51 and 0.25 Ti apfu at $z = 0$ and $z = 0.5$ layer, respectively. The latter result is compatible with a greater extent of the Ti-oxy component for the $z = 0$ layer as suggested by the analysis of diagnostic geometric parameters (see below). For such a reason, we consider the $C1$ as the most suitable space group for the description of the study crystal.

The oxy-type mechanism has been previously proposed by Schingaro et al. (2005) as the most likely for the entry of Ti in the structure of the $1M$ -BHG micas. As stated above, this appears also to

TABLE 8. Mean atomic numbers (electrons, e^-) of cation sites, octahedral and tetrahedral mean distances (Å), as determined by structure refinements (X-ref) in the $C\bar{1}$ and $C1$ space group and chemical analyses (EPMA)

	$C\bar{1}$	$C1$
$\langle T-O \rangle_{X-ref}$	1.658	1.657
$\langle T-O \rangle_{EPMA}$	1.657	1.657
$\langle M-O \rangle_{X-ref}$	2.085	2.086
$\langle M-O \rangle_{EPMA}$	2.079	2.079
$T e^-_{X-ref}$	13.87	13.97
$T e^-_{EPMA}$	13.71	13.71
$e^-_{(M1) X-ref}$	39.44	41.22
$e^-_{(M2) X-ref}$	36.78	37.62
$e^-_{(M1+2M2) X-ref}$	56.50	58.23
$e^-_{(M1+2M2) EPMA}$	56.75	56.75
$K e^-_{X-ref}$	19.36	19.51
$K e^-_{EPMA}$	18.16	18.16

Note: Average error for X-ref mean atomic numbers is $\pm 0.5 e^-/site$; EPMA mean atomic numbers are reproducible within $\pm 0.01 e^-$ for tetrahedral site, $\pm 0.4 e^-$ for octahedral site and $\pm 0.3 e^-$ for interlayer.

TABLE 9. Cation distribution for $C\bar{1}$ and $C1$ space groups

		e^-_{X-ref}	e^-_{EPMA}
Octahedral sheet			
$C\bar{1}$ space group			
Layer at $z = 0$	$(Mg_{2.54}Al_{0.30}Ti_{0.16})$	37.44	37.90
Layer at $z = 0.5$	$(Fe_{2.32}^{2+}Fe_{0.08}^{3+}Ti_{0.60})$	75.58	75.60
$C1$ space group			
Layer at $z = 0$	$(Mg_{2.49}Ti_{0.51})$	42.57	41.10
Layer at $z = 0.5$	$(Al_{0.30}^{3+}Mg_{0.05}Fe_{2.32}^{2+}Fe_{0.08}^{3+}Ti_{0.25})$	73.90	72.40
Tetrahedral sheet			
$C1$ space group			
Layer at $z = 0$	$(Si_{2.98}Al_{1.02})$	55.94	54.98
Layer at $z = 0.5$	$(Si_{2.72}Al_{1.28})$	55.82	54.72

Note: for errors associated to e^-_{X-ref} and e^-_{EPMA} see footnote of Table 8.

be the case of the $2M_1$ -BHG studied crystal. Three out of the most sensitive octahedral geometrical parameters reflective of the Ti-oxy mechanism are the $\langle M2-O4 \rangle$ distance, the $shift_{M2}$ parameter and the BLD_{M2} , bond-length distortion parameter of the M2 site (see Tables 7 and 10). Indeed, Figure 3 shows that the study crystal together with all the other literature $2M_1$ micas define rough a negative trend, as expected for micas interested by oxy mechanisms (Scordari et al. 2012; Lacalamita et al. 2011). Note that the average M2-O4 distance assumes different values for the $z = 0$ (2.015 Å) and $z = 0.5$ layers (2.024 Å), the lower the value the greater the amount of the oxy component. In Figure 4, the $shift_{M2}$ parameter becomes larger when the Ti-oxy component increases. For the study sample, the greatest $shift_{M2}$ value (on average 0.083 Å) for the $z = 0$ layer testifies for a stronger oxy component affecting this layer in comparison to that (on average 0.061 Å) at $z = 0.5$. In addition, the average BLD_{M2} parameter calculated for the $z = 0$ layer (2.215) is higher than that (1.718) obtained for the $z = 0.5$ layer (see Table 10). Also in this case the interpretation is straightforward if it is recalled that direct proportionality exists between the value of the BLD_{M2} parameter and the oxy component (Cruciani and Zanazzi 1994).

(2) The T sheets at $z = 0$ and $z = 0.5$ are quite homogeneous in composition. Indeed, only slight differences occur between the occupancies of the sites $T1$, $T1^{[1]}$, $T2$, and $T2^{[1]}$ on one side and $T1^{[2]}$, $T1^{[c]}$, $T2^{[2]}$, and $T2^{[c]}$ on the other side (see Table 6), the average distances $\langle T-O \rangle_{z=0}$ (1.653 Å) and $\langle T-O \rangle_{z=0.5}$ (1.661 Å) and the in plane ditrigonal angles, α (see Table 10). Accordingly, the tetrahedral cation distribution at $z = 0$ and $z = 0.5$ are

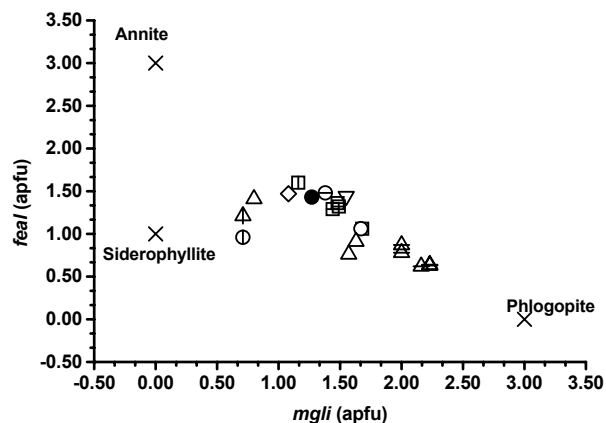


FIGURE 1. Chemical classification diagram modified after Scordari et al. (2012) including the study crystal and all the literature trioctahedral $2M_1$ micas belonging to the phlogopite-annite solid solution. $feal = (Fe_{tot} + Mn + Ti - ^{VI}Al)$; $mgli = (Mg-Li)$. Symbols: solid symbols = study crystal (circle: BHG); open symbols = igneous phlogopites from literature (square: Takeda and Ross 1975; circle: Ohta et al. 1982; pointing upward triangle: Bigi et al. 1993; pointing downward triangle: Bigi and Brigatti 1994; diamond: Brigatti et al. 2005); open symbols with horizontal line = other igneous phlogopites from literature (square: Laurora et al. 2007; circle: Pini et al. 2008; pointing upward triangle: Scordari et al. 2012); open symbols with vertical line = metamorphic phlogopites from literature (square: Bohlen et al. 1980; circle: Brigatti et al. 2000; pointing upward triangle: Brigatti et al. 2008).

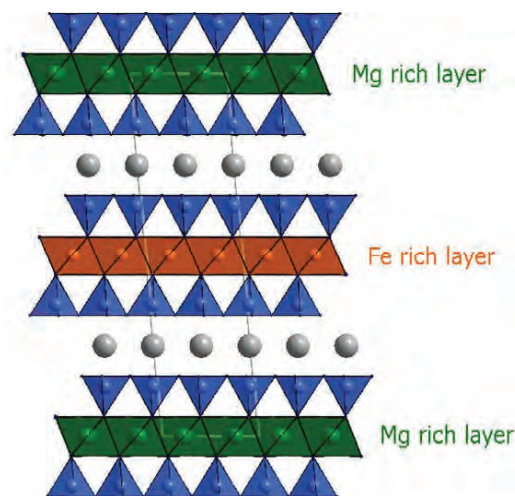


FIGURE 2. Representation of the $2M_1$ -BHG structure: the octahedral ordering at $z = 0$ and $z = 0.5$ layers is highlighted, according to the cation partition shown in Table 9. (Color online.)

fairly similar (see Table 9). To be more precise, on average, the tetrahedral sheet at $z = 0.5$ shows a slightly greater Al content than that at $z = 0$.

As mentioned above, the study $2M_1$ -BHG phlogopite has

TABLE 10. Selected distortional parameters from the structure refinements of the study crystal in the $C1$ space group

	$2M_1$ -BHG							
	Layer at $z = 0$				Layer at $z = 0.5$			
	T1 ^[1] _{lower}	T2 ^[1] _{lower}	T1 ^[1] _{upper}	T2 ^[1] _{upper}	T1 ^[2] _{lower}	T2 ^[2] _{lower}	T1 ^[c] _{upper}	T2 ^[c] _{upper}
BLD _T	1.024	0.469	1.419	1.071	0.800	1.209	0.819	1.487
V _T (Å ³)	2.331	2.328	2.302	2.313	2.296	2.325	2.402	2.373
TQE _T	1.001	1.001	1.001	1.001	1.001	1.000	1.001	1.001
TAV _T (°)	3.39	1.60	1.77	2.08	1.69	1.20	2.63	1.55
τ (°)	110.8	110.3	109.8	110.4	110.1	110.1	110.3	110.4
Δz _{lower} (Å)	0.060				0.008			
Δz _{upper} (Å)	0.040				0.028			
α _{lower} (°)	5.13				6.07			
α _{upper} (°)	6.27				5.71			
D.M. _{lower} (Å)	0.424				0.501			
D.M. _{upper} (Å)	0.442				0.507			
t _{tet} (Å) _{lower}	2.236				2.214			
t _{tet} (Å) _{upper}	2.207				2.284			
	M1				M1 ^[2]			
ψ _{M1} (°)	58.18				58.82			
BLD _{M1}	3.629				1.312			
V _{M1} (Å ³)	12.410				12.063			
OQE _{M1}	1.015				1.015			
OAV _{M1} (°)	44.78				48.52			
ELD _{M1}	4.974				5.683			
e _s M1/e _s M1	1.105				1.122			
	M2		M2 ^[1]		M2 ^[2]		M2 ^[c]	
ψ _{M2} (°)	57.80	57.34			58.21	57.37		
BLD _{M2}	3.194	1.236			2.271	1.165		
ELD _{M2}	4.568	4.062			5.053	5.204		
V _{M2} (Å ³)	12.070	11.674			11.504	11.621		
OQE _{M2}	1.012	1.008			1.012	1.012		
OAV _{M2} (°)	35.99	24.49			38.87	40.41		
e _s M2/e _s M2	1.096	1.085			1.106	1.110		
Shift _{M2} (Å)	0.122	0.043			0.080	0.041		
t _{oct} (Å)	2.233				2.174			
t _{int} (Å)	3.383				3.364			
Δ _{K-O} (Å)	0.274				0.256			
t _{K-O4} Lower (Å)	3.980				3.996			
t _{K-O4} Upper (Å)	3.970				3.953			

Notes: Superscript ^[2] indicates atomic position obtained by the twofold symmetry operation; superscript ^[1] indicates atomic position obtained by inversion center; superscript ^[c] indicates atomic position obtained by c-glide; subscript "lower" indicates the lower tetrahedral layer of a TOT unit; subscript "upper" indicates the upper tetrahedral layer of a TOT unit. t_{tet}: tetrahedral sheet thickness calculated from z coordinates of basal and apical O atoms; TQE: tetrahedral quadratic elongation (Robinson et al. 1971); TAV: tetrahedral angle variance (Robinson et al. 1971); τ: tetrahedral flattening angle; α: tetrahedral rotation angle (Hazen and Burnham 1973); Δz: departure from complanarity of the basal O atoms (Güven 1971); D.M.: dimensional mismatch between tetrahedral and octahedral sheets (Toraya 1981); ψ: octahedral flattening angles (Donnay et al. 1964a, 1964b); BLD: bond-length distortions (Renner and Lehmann 1986); ELD: edge-length distortion (Renner and Lehmann 1986); Shift_{M2}: off-center shift of the M2 cation defined as the distance between the M2 cation and the polyhedron centroid; OQE: octahedral quadratic elongation (Robinson et al. 1971); OAV: octahedral angle variance (Robinson et al. 1971); e_s, e_s: mean lengths of unshared and shared edges, respectively (Toraya 1981); t_{oct}: octahedral sheet thickness (Toraya 1981); t_{int}, calculated from the z coordinates of basal O atoms; Δ_{K-O} = <K-O>_{outer} - <K-O>_{inner}; t_{K-O4}: projection of K-O4 distance along c*. Errors on distortion parameters, estimated by varying the refined positional parameters within one standard deviation, are in the following ranges: <0.5% for volumes, thicknesses, projected bond lengths, shifts; 0.1–13% for angles, bond/edge lengths distortions, sheet corrugations, D.M., Δ_{K-O}.

been found in coexistence in the same rock sample with a $1M$ polytype (Schingaro et al. 2005). By comparing the $1M$ - and $2M_1$ -BHG structures in the $2M_1$ setting (space group $C2/c$), it is easily calculated that the only significant differences between atomic positions are those relevant to the y coordinate of the O31, O32, and O4 oxygen atoms (the absolute value of $\Delta y_{O31,O32} = 0.012$, $\Delta y_{O4} = 0.013$). Analogous values calculated by Takeda and Ross (1975) for their $1M$ and $2M_1$ coexisting biotite are $\Delta y_{O31,O32,O4} = 0.009$. As also previously reported by these authors,

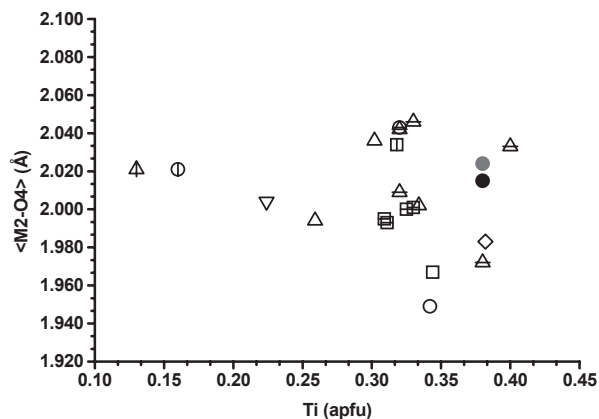


FIGURE 3. <M2-O4> distance vs. Ti content plot. Symbols as in Figure 1. Black solid symbol = $2M_1$ -BHG sample at $z = 0$; gray solid symbol = $2M_1$ -BHG sample at $z = 0.5$.

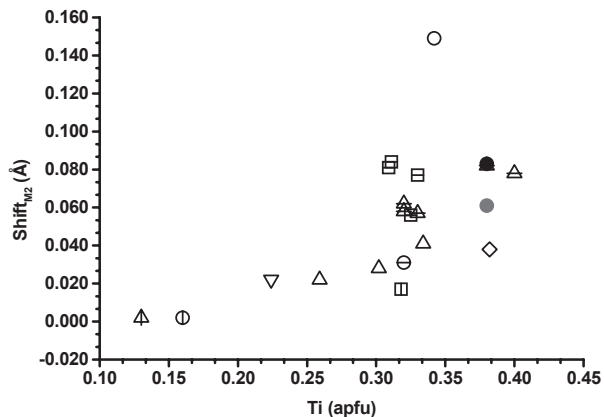


FIGURE 4. Shift_{M2} parameter vs. Ti content plot modified after Scordari et al. (2012). Symbols as in Figure 1. Black solid symbol = $2M_1$ -BHG sample at $z = 0$; gray solid symbol = $2M_1$ -BHG sample at $z = 0.5$.

the symmetry lowering shown by the study $2M_1$ phlogopite may be a consequence of the $2M_1$ layer stacking, which affects the position of the octahedral oxygen atoms along the $\pm b$ direction. However, the symmetry lowering of the study crystal may be also due to the octahedral cation ordering. In a very recent paper on the coexistence of $1M$ - and $2M_1$ -polytypes, it was hypothesized that the probability of occurrence of $2M_1$ polytype depends on the degree of cation ordering at octahedral sites but may be also related to the extent of oxy-type substitutions that destabilize the octahedral sheet (Lacalamita et al. 2012). All the $2M_1$ -phlogopites reported to date in literature are completely (Ohta et al. 1982; Laurora et al. 2007; BU1_8, BU1_14, and BU1_16 crystals from Lacalamita et al. 2012) or partially (Takeda and Ross 1975; Bigi and Brigatti 1994; Brigatti et al. 2008; BU1_15 and BU1_17 crystals from Lacalamita et al. 2012) disordered at octahedral sites. Also the $1M$ -BHG polytype coexisting with the study sample show disordered cation distribution at octahedral sites, apart from the partial ordering (Ti at M2 site) directly caused by the Ti-oxy substitution. The peculiarity of the studied $2M_1$ -

polytype stems from the remarkable ordering of the octahedral layers, that results in the c cell parameter becoming twice as that of the $1M$ -BHG in Schingaro et al. (2005), as well as in notably different chemical composition of the $z = 0$ and $z = 0.5$ layers. The results point to the description of the present samples as a “configurational polytype” (Ferraris et al. 2004). Really, with respect to the strict definition of polytypes, characterized by constant or nearly constant composition (up to 0.25 atoms per formula unit) of the stacking layers (Bailey 1984; Guinier et al. 1984), configurational polytypes have been described as having the same layer configuration and layer-stacking principle, but radically different chemical compositions (Makovicky 1997; Ferraris et al. 2004).

ACKNOWLEDGMENTS

The authors thank Marcello Serracino for assistance during electron probe microanalyses at the CNR-Istituto di Geologia Ambientale e Geoingegneria (Roma). Maria Franca Brigatti is acknowledged for supplying the mica sample. Helpful reviews by Stuart Mills and two anonymous referees improved the paper. This work was funded by the COFIN-MIUR.

REFERENCES CITED

- Bailey, S.W. (1984) Crystal chemistry of the true micas. In S.W. Bailey, Ed., *Micas*, 13, 13–61. Reviews in Mineralogy, Mineralogical Society of America, Chantilly, Virginia.
- Betteridge, P.W., Carruthers, J.R., Cooper, R.I., Prout, K., and Watkin, D.J. (2003) Crystals version 12: software for guided crystal structure analysis. *Journal of Applied Crystallography*, 36, 1487.
- Bigi, S. and Brigatti, M.F. (1994) Crystal chemistry and microstructures of plutonic biotite. *American Mineralogist*, 79, 63–72.
- Bigi, S., Brigatti, M.F., Mazzucchelli, M., and Rivalenti, G. (1993) Crystal chemical variations in Ba-rich from gabbroic rocks of lower crust (Ivrea Zone, NW Italy). *Contributions to Mineralogy and Petrology*, 113, 87–99.
- Bohlen, S.R., Peacor, D.R., and Essene, E.J. (1980) Crystal chemistry of a metamorphic biotite and its significance in water barometry. *American Mineralogist*, 65, 55–62.
- Brigatti, M.F. and Guggenheim, S. (2002) Mica crystal chemistry and the influence of pressure, temperature, and solid solution on atomistic models. In A. Mottana, F.P. Sassi, J.B. Thompson Jr., and S. Guggenheim, Eds., *Micas: Crystal Chemistry & Metamorphic Petrology*, 46, 1–97. Reviews in Mineralogy and Geochemistry, Mineralogical Society of America and the Geochemical Society, Chantilly, Virginia.
- Brigatti, M.F., Frigieri, P., Ghezzi, C., and Poppi, L. (2000) Crystal chemistry of Al-rich biotites coexisting with muscovites in peraluminous granites. *American Mineralogist*, 85, 436–448.
- Brigatti, M.F., Caprilli, E., Funicello, R., Giordano, G., Mottana, A., and Poppi, L. (2005) Crystal chemistry of ferroan phlogopites from the Albano maar lake (Colli Albani volcano, central Italy). *European Journal of Mineralogy*, 17, 611–621.
- Brigatti, M.F., Guidotti, C.V., Malferrari, D., and Sassi, F.P. (2008) Single-crystal X-ray studies of trioctahedral micas coexisting with dioctahedral micas in metamorphic sequences from western Maine. *American Mineralogist*, 93, 396–408.
- Bruker (2003a) APEX2. Bruker AXS Inc., Madison, Wisconsin, U.S.A.
- (2003b) SAINT. Bruker AXS Inc., Madison, Wisconsin, U.S.A.
- Bujnowski, T., Guggenheim, S., and Kato, T. (2009) Crystal structure determination of anandite- $2M$ mica. *American Mineralogist*, 94, 1144–1152.
- Castle, J.E. and Salvi, A.M. (2001) Chemical state information from the near-peak region of the X-ray photoelectron background. *Journal of Electron Spectroscopy*, 114–116, 1103–1113.
- Cruciani, G. and Zanazzi, P.F. (1994) Cation partitioning and substitution mechanisms in $1M$ phlogopite: A crystal chemical study. *American Mineralogist*, 79, 289–301.
- Donnay, G., Morimoto, N., Takeda, H., and Donnay, J.D.H. (1964a) Trioctahedral one-layer micas. I. Crystal structure of a synthetic iron mica. *Acta Crystallographica*, 17, 1369–1373.
- Donnay, G., Donnay, J.D.H., and Takeda, H. (1964b) Trioctahedral one-layer micas. II. Prediction of the structure from composition and cell dimensions. *Acta Crystallographica*, 17, 1374–1381.
- Ferraris, G., Makovicky, E., and Merlino, S. (2004) Crystallography of modular materials. *International Union of Crystallography Monographs on Crystallography*, 15, 207–226. Oxford Science, U.K.
- Foley, S.F. (1989) Experimental constraints of phlogopite chemistry in lamproites; 1. The effect of water activity and oxygen fugacity. *European Journal of Mineralogy*, 1, 411–426.
- Guinier, A., Bokij, G.B., Boll-Domberger, K., Cowley, J.M., Đurović, S., Jagodzinski, H., Krishna, P., de Wolff, P.M., Zvyagin, B.B., Cox, D.E., Goodman, P., Hahn, T., Kuchitsu, K., and Abrahams, S.C. (1984) Nomenclature of polytype structures. Report of the International Union of Crystallography *Ad hoc* Committee on the Nomenclature of Disordered, Modulated and Polytype Structures. *Acta Crystallographica*, A, 40, 399–404.
- Güven, N. (1971) The crystal structure of $2M_1$ phengite and $2M_1$ muscovite. *Zeitschrift für Kristallographie*, 134, 196–212.
- Hawthorne, F.C., Ungaretti, L., and Oberti, R. (1995) Site populations in minerals: terminology and presentation of results of crystal-structure refinement. *Canadian Mineralogist*, 33, 907–911.
- Hazen, R.M. and Burnham, C.W. (1973) The crystal structures of one-layer phlogopite and annite. *American Mineralogist*, 58, 889–900.
- Lacalamita, M., Schingaro, E., Scordari, F., Ventruti, G., Fabrizio, A., and Pedrazzi, G. (2011) Substitution mechanisms and implication on the estimate of water fugacity for Ti-phlogopite from Mt. Vulture (Potenza, Italy). *American Mineralogist*, 96, 1381–1391.
- Lacalamita, M., Mesto, E., Scordari, F., and Schingaro, E. (2012) Chemical and structural comparison of $1M$ - and $2M_1$ -phlogopites coexisting in the same Kasenyi kamafugitic rock (SW Uganda). *Physics and Chemistry of Minerals*, 39, 601–611, DOI: 10.1007/s00269-012-0515-y.
- Lahti, S.I. and Saikkonen, R. (1985) Bityite $2M_1$ from Eräjärvi compared with related Li-Be brittle micas. *Bulletin of the Geological Society of Finland*, 57, 207–215.
- Laurora, A., Brigatti, M.F., Mottana, A., Malferrari, D., and Caprilli, E. (2007) Crystal chemistry of trioctahedral micas in alkaline and subalkaline volcanic rocks: A case study from Mt. Sassetto (Tolfa district, Latium, central Italy). *American Mineralogist*, 92, 468–480.
- Lin, J.-C. and Guggenheim, S. (1983) The crystal structure of a Li, Be-rich brittle mica: a dioctahedral-trioctahedral intermediate. *American Mineralogist*, 68, 130–142.
- Makovicky, E. (1997) Prediction of modular crystal structures. In H. Burzlaff, Ed., *Proceeding Symposium on Predictability of Crystal Structures of Inorganic Solids*, Hünfeldt 27.10–30.10.1997. Erlangen: Universität Erlangen-Nürnberg, p. 107–124.
- Mesto, E., Scordari, F., Guascito, M.R., and Malitesta, C. (2008) Appraisal of Ti speciation in trioctahedral micas by means of XPS investigation: recent improvements and applications. 1st SIMP-AIC Joint Meeting, Sestri Levante, 7–12 September 2008, Programme and Book of Abstract, 83.
- Ohta, T., Takeda, H., and Takéuchi, Y. (1982) Mica polytypism: similarities in the crystal structures of coexisting $1M$ and $2M_1$ oxybiotite. *American Mineralogist*, 67, 298–310.
- Pini, S., Affronte, M., and Brigatti, M.F. (2008) Magnetic behaviour of trioctahedral mica- $2M_1$ occurring in a magnetic anomaly zone. *Mineralogical Magazine*, 72, 1035–1042.
- Pouchou, J.L. and Pichoir, F. (1985) “PAP” $\Phi(\rho Z)$ procedure for improved quantitative microanalysis. In J.T. Armstrong, Ed., *Microbeam Analysis*, 104–106. San Francisco Press, California.
- Renner, B. and Lehmann, G. (1986) Correlation of angular and bond length distortions in TO_4 units in crystals. *Zeitschrift für Kristallographie*, 175, 43–59.
- Rieder, M., Hybler, J., Smrčok, L.U., and Weiss, Z. (1996) Refinement of the crystal structure of zinnwaldite $2M_1$. *European Journal of Mineralogy*, 8, 1241–1248.
- Robinson, K., Gibbs, G.V., and Ribbe, P.H. (1971) Quadratic elongation: A quantitative measure of distortion in coordination polyhedra. *Science*, 172, 567–570.
- Schingaro, E., Scordari, F., Mesto, E., Brigatti, M.F., and Pedrazzi, G. (2005) Cation site partitioning in Ti-rich micas from Black Hill (Australia): A multi-technical approach. *Clays and Clay Minerals*, 53, 179–189.
- Scordari, F., Schingaro, E., Lacalamita, M., and Mesto, E. (2012) Crystal chemistry of trioctahedral micas- $2M_1$ from Bunyaruguru (SW Uganda) kamafugite. *American Mineralogist*, 97, 430–439.
- Shannon, R.D. (1976) Revised effective ionic radii and systematic studies of interatomic distances in halides and chalcogenides. *Acta Crystallographica*, A, 32, 751–767.
- Sheldrick, G.M. (2003) SADABS, Program for Empirical Absorption Correction of Area Detector Data. University of Göttingen, Germany.
- Slade, P.G., Schultz, P.K., and Dean, C. (1987) Refinement of the ephesite structure in $C1$ symmetry. *Neues Jahrbuch für Mineralogie Monatshefte*, 6, 275–287.
- Swanson, T.H. and Bailey, S.W. (1981) Redetermination of the lepidolite- $2M_1$ structure. *Clays and Clay Minerals*, 29, 81–90.
- Takeda, H. and Ross, M. (1975) Mica polytypism: Dissimilarities in the crystal structures of coexisting $1M$ and $2M_1$ biotite. *American Mineralogist*, 60, 1030–1040.
- Toraya, H. (1981) Distortions of octahedra and octahedral sheets in $1M$ micas and the relation to their stability. *Zeitschrift für Kristallographie*, 157, 173–190.
- Turner, S.P. (1996) Petrogenesis of the late-Delamerian gabbroic complex at Black Hill, South Australia: Implications for convective thinning of the lithospheric mantle. *Mineralogy and Petrology*, 56, 51–89.